Marc Hodes[1]
Department of Mechanical Engineering,
Tufts University,
Medford, MA 02155
e-mail: marc.hodes@Tufts.edu

Lisa Steigerwalt Lam
Department of Mechanical Engineering,
Tufts University,
Medford, MA 02155
e-mail: lisa_lam@alum.mit.edu

Adam Cowley
Department of Mechanical Engineering,
Brigham Young University,
Provo, UT 84602
e-mail: adam.m.cowley@gmail.com

Ryan Enright
Thermal Management Research Group,
Efficient Energy Transfer (ηet) Department,
Bell Labs Ireland,
Alcatel-Lucent Ireland Ltd.,
Blanchardstown Business & Technology Park,
Dublin 15, Ireland
e-mail: ryan.enright@alcatel-lucent.com

Scott MacLachlan
Department of Mathematics and Statistics,
Memorial University of Newfoundland,
St Johns, NL A1C 5S7, Canada
e-mail: smaclachlan@mun.ca

Effect of Evaporation and Condensation at Menisci on Apparent Thermal Slip

We semi-analytically capture the effects of evaporation and condensation at menisci on apparent thermal slip lengths for liquids suspended in the Cassie state on ridge-type structured surfaces using a conformal map and convolution. An isoflux boundary condition is prescribed at solid–liquid interfaces and a constant heat transfer coefficient or isothermal one at menisci. We assume that the gaps between ridges, where the vapor phase resides, are closed systems; therefore, the net rates of heat and mass transfer across menisci are zero. The reduction in apparent thermal slip length due to evaporation and condensation relative to the limiting case of an adiabatic meniscus as a function of solid fraction and interfacial heat transfer coefficient is quantified in a single plot. The semi-analytical solution method is verified by numerical simulation. Results suggest that interfacial evaporation and condensation need to be considered in the design of microchannels lined with structured surfaces for direct liquid cooling of electronics applications and a quantitative means to do so is elucidated. The result is a decrease in thermal resistance relative to the predictions of existing analyses which neglect them.
[DOI: 10.1115/1.4029818]

Keywords: heat transfer, apparent thermal slip length, evaporation, condensation

1 Introduction

A sessile droplet on a structured surface characterized by periodic length scales that are small compared to the capillary length may be stable in the Cassie state, where solid–liquid contact is confined to the tips of the structures [1]. A liquid flowing over a structured surface may also be in this state, which we assume here and depict in Fig. 1 for ridge-type structures. The necessary criteria are provided elsewhere [2]. The solid–liquid interface is subjected to the no-slip boundary condition, but lubrication is achievable because low shear stress may be maintained at the meniscus (liquid–vapor interface). Heat is supplied to the liquid primarily through the solid–liquid interface.

Trapping a flowing liquid in the Cassie state is envisioned for enhanced microchannel cooling of electronics [2,3]. This reduces the caloric resistance, $1/(\dot{m}c_p)$, to heat transfer, but, simultaneously, degrades the effective heat transfer coefficient. To evaluate the efficacy of the enhancement it is necessary to capture the beneficial effects of condensation and evaporation along menisci on reducing apparent thermal slip length when a volatile coolant such as water is utilized.

We consider a periodic array of ridges of width $2a$, of pitch $2d$, and centered about the origin and assume that menisci are flat as per the semi-infinite domain shown in Fig. 2. The composite interface corresponds to the $y=0$ boundary of the domain and includes the solid–liquid interface and the meniscus. Solid fraction (ϕ) equals the area fraction of the solid–liquid portion of the composite interface, a/d. The temperature field is symmetric about $x=0$ and $x=d$. We assume that the gaps between ridges, where the vapor phase resides, are closed systems.[2] This is true, when, e.g., ridges reside in a trench on a substrate over which liquid flows. We consider steady-state conditions; therefore, the net rates of heat and mass transfer into the meniscus are zero. Thermophysical properties are assumed to be constant.

The Reynolds number characterizing flow near a composite interface in the limit as solid fraction approaches zero is $\mathrm{Re}_c = \rho \bar{w}_c a/\mu$, where w is streamwise velocity, the overbar denotes a mean quantity, the subscript c denotes the composite interface, and ρ and μ are liquid density and viscosity, respectively. More generally, Re_c cannot exceed $\rho \bar{w}_c d/\mu$. The corresponding Péclet number is $\mathrm{Pe}_c = \mathrm{Re}_c\mathrm{Pr}$, where Pr is the Prandtl number of the liquid. At pitches characterizing structured surfaces, Re_c and Pe_c approach zero in most applications. Thus, as we assume here, viscous dissipation is negligible, transport is diffusive, and the temperature field is governed by Laplace's equation for the "inner problem."

There is a distinction between the true temperature profiles, $T(x,y,z)$ and $T(x,y)$ for ridges oriented parallel and transverse to the streamwise direction, respectively, and those averaged over the width of the domain, d, $\bar{T}(y,z)$ and $\bar{T}(y)$ for parallel and transverse ridges, respectively. However, the (maximum) length scale for the distance normal to the composite interface to which it applies is d. We assume that length scales characterizing the "outer problem," e.g., boundary layer thickness in an external flow, are large compared to d. Then, heat flux is constant as

[1]Corresponding author.

Contributed by the Heat Transfer Division of ASME for publication in the Journal of Heat Transfer. Manuscript received July 30, 2014; final manuscript received February 5, 2015; published online March 24, 2015. Assoc. Editor: Giulio Lorenzini.

[2]The "vapor" phase normally has vapor and noncondensable gas components.

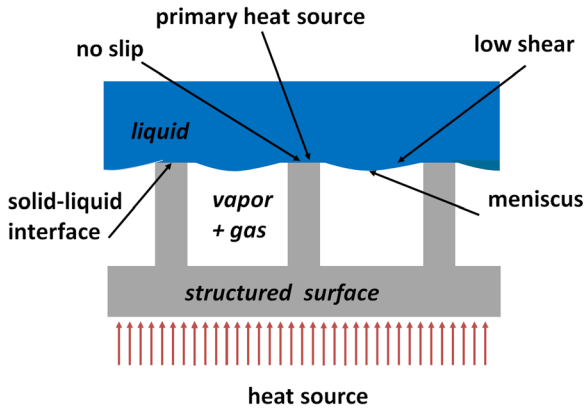

Fig. 1 Liquid in Cassie state on ridge-type structures

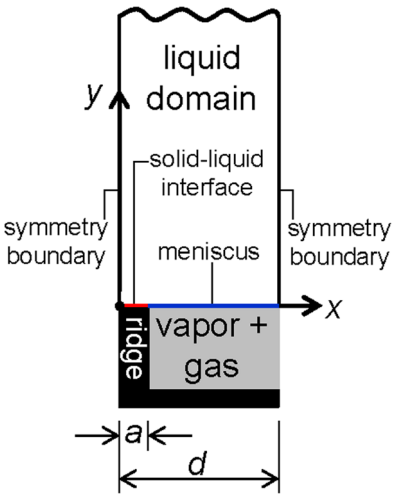

Fig. 2 Liquid domain and ridge and vapor region beneath it

$y \to \infty$ in the inner problem, as it is within the linear region of the temperature profile of the outer one. We further assume that $\partial^2 T/\partial x^2 \sim \partial^2 T/\partial y^2 \gg \partial^2 T/\partial z^2$ in the inner problem such that it is governed by the two-dimensional form of the Laplace equation. This is precisely true for a fully developed internal flow over parallel ridges subjected to a constant heat flux at the solid–liquid interface (q''_{sl}). However, our analysis assumes symmetry boundary conditions in x; therefore, it only applies to flow over transverse ridges when the linear component of the streamwise temperature change may be ignored. The preceding discussion is restricted to laminar flows due to the minute length scales associated with viscous sublayers in turbulent flows.

Apparent slip results from the interaction of liquid flow with regions of solid–liquid contact and menisci. The no-slip boundary condition applies at solid–liquid interfaces, but not along menisci; therefore, lubrication may be realized in microfluidic conduits. The apparent hydrodynamic slip length (b), subsequently referred to as the slip length, relates the streamwise velocity averaged over the width of the domain to its gradient at the composite interface as per [4]

$$\bar{w}_c = b \left.\frac{\partial \bar{w}}{\partial y}\right|_c \tag{1}$$

Analogously, the apparent thermal slip length (b_t), also referred to as the temperature jump length and subsequently referred to as the thermal slip length, relates the difference between the mean temperatures of the solid–liquid and composite interfaces to the gradient of $\bar{T}(y)$ at the composite interface as per

$$\bar{T}_{sl} - \bar{T}_c = -b_t \left.\frac{\partial \bar{T}}{\partial y}\right|_c \tag{2}$$

where the subscript sl denotes the solid–liquid interface, where a constant heat flux is prescribed. (Thermal slip length may also be based upon the maximum temperature of the solid–liquid interface.) We note that as per the Leibniz Rule $\partial \bar{T}/\partial y|_c$ equals the mean heat flux at the composite interface scaled by the thermal conductivity of the liquid which, in turn, as per an energy balance on the domain equals $dT/dy|_{y\to\infty}$.

Slip lengths and thermal slip lengths often follow from the solution to the inner problems and capture perturbations to the velocity and temperature fields due to structured surfaces. Assuming a flat and shear-free meniscus, expressions for slip length were developed by Lauga and Stone [5] for parallel and transverse ridges and by Davis and Lauga [6] and Enright et al. [7] for pillars.[3] More generally, Ybert et al. [8] developed scaling laws that consider meniscus curvature and viscous dissipation in the gas phase.

Analytical results for thermal slip length for isoflux and isothermal solid–liquid interfaces and adiabatic menisci were developed by Enright et al. [7] for ridge- and pillar-type structures based upon expressions for thermal spreading resistances [9]. Ng and Wang [10] semi-analytically computed thermal slip lengths for isothermal, ridge-type structures as a function of vapor phase to liquid-phase thermal conductivity and ridge depth when isothermal surfaces bounded the vapor phase. When the cavity depth is shallow compared to structure spacing, conduction through the vapor phase can reduce the thermal slip length relative to the case of an adiabatic meniscus. For cavity depths on the order of the spacing of the structures and larger, conduction through the gas has negligible impact on slip length. No effort is made to account for this effect here. Ng and Wang [10] also semi-analytically computed slip lengths for an isothermal surface with adiabatic circular or square holes. The preceding results are based on pure diffusion in the aforementioned inner problem. Maynes and Crockett [11] analytically studied Poiseuille flow in a parallel plate channel lined with parallel ridges subjected to a constant heat flux by solving the thermal energy equation rather than the Laplace equation, thereby accounting for advection. They developed a closed form solution for the local Nusselt number in agreement with Enright et al. [7] and provided an expression for thermal slip length based on it. Finally, Cowley et al. [12] account for the effects of axial conduction in a numerical study of Poiseuille flow in a parallel plate channel lined with transverse ridges. Their results elucidate when axial conduction is important and when diffusion-based analyses apply as a function of the relevant dimensionless parameters.

We capture the effects of evaporation and condensation along the meniscus on thermal slip length, when the tips of ridge-type structures are isoflux. Significantly, when heat is transferred from the solid–liquid interface into the liquid, evaporation occurs along the relatively hot portion of the meniscus adjacent to the triple contact line and condensation elsewhere. Therefore, a fraction of the heat entering the domain conducts through the liquid to the relatively hot portion of the meniscus, drives evaporation, convects through the vapor phase and is transported back into the liquid by condensation. This decreases thermal slip length relative to the limiting case of an adiabatic meniscus, except in the case of a nonvolatile liquid, e.g., galinstan. This has ramifications on the efficacy of using structured surfaces to reduce the thermal resistance of microchannel cooling of microelectronics [2].

In the general case, we prescribe solid fraction and the dimensionless interfacial heat transfer coefficient at the meniscus, $\tilde{h}$. Then, the limiting case of an isothermal meniscus ($\tilde{h} \to \infty$) is

[3]For pillar-geometry structures, the velocity and temperature fields in the inner problems are three-dimensional; therefore, velocities and temperatures are averaged over areas rather than line segments to compute slip lengths.

addressed. We note that thermal slip lengths are geometric parameters only in the limits of an adiabatic or isothermal meniscus.

Macroscopic parameters, e.g., Poiseuille and Nusselt numbers, follow by imposing the boundary conditions given by Eqs. (1) and (2) on the convective transfer equations governing the outer problem. These govern the velocity and temperature fields averaged over the appropriate length (e.g., ridge pitch) or area (e.g., that bounded by symmetry lines surrounding a pillar); see, e.g., Steigerwalt Lam et al. [13]. By implication, the Nusselt number is a function of the thermal slip length, and its value computed from the analysis herein rather than that for an adiabatic meniscus should be utilized. Subsequently, a microchannel heat sink exploiting the favorable effects of liquid flowing over textured surfaces may be optimized as per the analysis of Steigerwalt Lam et al. [13].

We note that when the Knudsen number characterizing an internal gas flow is between about 0.001 and 0.01 the continuum forms of the convective transfer equations apply, but the wall boundary conditions which account for molecular slip are of the same form as Eqs. (1) and (2) [14]. Therefore, expressions in the rarefied gas and microflow literature for Poiseuille number (see, e.g., Duan and Muzychka [15]) and Nusselt number (see, e.g., Colin [16]) apply to liquid flows exhibiting apparent slip. In both classes of problems, the effects of slip vanish as the ratio of the slip length to the length scale for the outer problem approaches zero. Hence, since apparent slip lengths scale with structure pitch [8], itself on the order of microns, apparent slip is relevant in laminar microchannel flows and turbulent flows [17].

2 Analysis

We organize this section according to the type of boundary condition imposed at the meniscus. First, we consider it adiabatic. Then, we prescribe a finite heat transfer coefficient. Finally, we consider it isothermal. The solid–liquid interface is isoflux.

2.1 Adiabatic Meniscus. As per the result of Enright et al. [7], for an adiabatic meniscus, dimensionless thermal slip length, $\tilde{b}_t = b_t/(2d)$, is

$$\tilde{b}_t = \frac{1}{\pi^3 \phi^2} \sum_{n=1}^{\infty} \frac{\sin^2(n\pi\phi)}{n^3} \tag{3}$$

2.2 Finite Heat Transfer Coefficient at Meniscus. The two-dimensional temperature field is governed by Laplace's equation

$$\nabla^2 T = 0 \tag{4}$$

subjected to

$$\frac{\partial T}{\partial y} = -\frac{q''_{sl}}{k} \quad \text{for} \quad 0 < x < a, \quad y = 0 \tag{5}$$

$$\frac{dT}{dy} = -\frac{a}{d}\frac{q''_{sl}}{k} \quad \text{for} \quad 0 < x < d, \quad y \to \infty \tag{6}$$

$$\frac{\partial T}{\partial y} = \frac{h}{k}(T - \bar{T}_{lv}) \quad \text{for} \quad a < x < d, \quad y = 0 \tag{7}$$

$$\frac{\partial T}{\partial x} = 0 \quad \text{for} \quad x = 0, \quad y > 0 \tag{8}$$

$$\frac{\partial T}{\partial x} = 0 \quad \text{for} \quad x = d, \quad y > 0 \tag{9}$$

where $\bar{T}_{lv}$ is the mean temperature of the meniscus and k is the thermal conductivity of the liquid. Implicit in the assignment of Eq. (7) to the meniscus is the assumption of a uniform pressure on the vapor side of it that corresponds to the saturation pressure associated with $\bar{T}_{lv}$. While local evaporation and condensation occur, the net heat and mass flows across the meniscus are zero. Hence, all the heat entering the domain at the solid–liquid interface is removed by the sensible temperature rise of the liquid, and the rate of heat leaving the domain as $y \to \infty$ equals that through the solid–liquid interface as per Eq. (6). Therefore, we develop the dimensionless parameter that must be small compared to unity to justify ignoring the heat advected out of the domain. Accordingly, we consider the domain shown in Fig. 2, with the exception that it is finite rather than semi-infinite. Its height is d, the maximum length scale required for the temperature field to become uniform in x in the inner problem, and it is of depth dz. For fully developed flow, the rate of heat advected out of the domain is

$$q_{adv} = \dot{m}_{inner} c_p \frac{dT_m}{dz} dz \tag{10}$$

where $\dot{m}_{inner}$ is the mass flow rate of liquid through the aforementioned (finite) inner domain, c_p is the specific heat of the liquid at constant pressure and T_m is the bulk temperature of the liquid. The characteristic velocity in the inner problem is that at $y = 0$, which equals $\overline{w}_c$ as per Eq. (1) and is readily computed from available expressions for b. Hence, $\dot{m}_{inner}$ is of order $\rho \overline{w}_c d^2$. Moreover, because the boundary condition at $y = 0$ is one of constant heat input, a macroscopic energy balance on a domain that extends across a parallel plate channel yields $dT_m/dz = 2q''_{sl}a/(\dot{m}c_p)$, where the factor of two implies that the channel is symmetrically heated and $\dot{m}$ is the total mass flow rate of liquid through the channel, which may be computed based upon available friction factors which account for hydrodynamic slip. It follows that

$$q_{adv} = \frac{2\rho \bar{w}_c d^2 q''_{sl} a}{\dot{m}} dz \tag{11}$$

The rate of heat conducted into the domain is $q''_{sl} a dz$ such that the criterion for negligible advection out of the domain becomes

$$\frac{2\rho \bar{w}_c d^2}{\dot{m}} \lesssim 0.1 \tag{12}$$

Physically, this implies that the mass flow rate of liquid through the inner portion of the domain is small compared to the total mass flow rate. We assume that Eq. (12) holds and proceed by neglecting the effects of heat advected out of the domain.

In dimensionless form, Laplace's equation becomes

$$\frac{\partial^2 \theta}{\partial \tilde{x}^2} + \frac{\partial^2 \theta}{\partial \tilde{y}^2} = 0 \tag{13}$$

where $\theta = (T - \bar{T}_{lv})k/(q''_{sl}d)$. Throughout this paper, variables with units of length are nondimensionalized by half of the pitch of the ridges (d) when a tilde symbol is placed over them. The exception is b_t, which is nondimensionalized by structure pitch ($2d$) to be consistent with most of the previous literature. The boundary conditions become

$$\frac{\partial \theta}{\partial \tilde{y}} = -1 \quad \text{for} \quad 0 < \tilde{x} < \phi, \quad \tilde{y} = 0 \tag{14}$$

$$\frac{\partial \theta}{\partial \tilde{y}} = \tilde{h}\theta \quad \text{for} \quad \phi < \tilde{x} < 1, \quad \tilde{y} = 0 \tag{15}$$

$$\frac{d\theta}{d\tilde{y}} = -\phi \quad \text{for} \quad 0 < \tilde{x} < 1, \quad \tilde{y} \to \infty \tag{16}$$

$$\frac{\partial \theta}{\partial \tilde{x}} = 0 \quad \text{for} \quad \tilde{x} = 0, \quad \tilde{y} > 0 \tag{17}$$

$$\frac{\partial \theta}{\partial \tilde{x}} = 0 \quad \text{for} \quad \tilde{x} = 1, \quad \tilde{y} > 0 \tag{18}$$

where $\tilde{h} = hd/k$. The symmetry boundary conditions in Eqs. (17) and (18) always apply, but are only explicitly stated here.

We homogenize the boundary condition given by Eq. (14) by defining $\tilde{u}(\tilde{x},\tilde{y}) = \tilde{\theta}(\tilde{x},\tilde{y}) + \tilde{y}$. Then, we conformally map the problem to the complex plane according to [18]

$$\tilde{v} = \frac{2}{\pi}\cos^{-1}\left[\frac{\cos(\pi\tilde{z}/2)}{\cos(\pi\phi/2)}\right] \tag{19}$$

where $\tilde{v} = \tilde{r}(\tilde{x},\tilde{y}) + i\tilde{s}(\tilde{x},\tilde{y})$ and $\tilde{z} = \tilde{x} + i\tilde{y}$. Equation (13) is preserved, but the independent variables become $\tilde{r}$ and $\tilde{s}$. The map sends the points $(0,\infty)$, $(0,0)$, $(\phi,0)$, $(1,0)$, and $(1,\infty)$ in the real $(\tilde{x},\tilde{y})$ plane to $(0,\infty)$, $(0,\tilde{D})$, $(0,0)$, $(1,0)$, and $(1,\infty)$, respectively, in the complex $(\tilde{r},\tilde{s})$ plane, where

$$\tilde{D} = \frac{2}{\pi}\ln\left[\frac{\cos(\pi\phi/2)}{1-\sin(\pi\phi/2)}\right] \tag{20}$$

Because $\tilde{D}$ is a finite, positive constant, the problem in the complex plane has a homogeneous Neumann boundary condition along $\tilde{r} = 0$ for $\tilde{s} > 0$. Also, the homogeneous Neumann boundary condition along $\tilde{x} = 1$ for $\tilde{y} > 0$ becomes one of the same type along $\tilde{r} = 1$ for $\tilde{s} > 0$. The nonhomogeneous Robin boundary condition along $\tilde{y} = 0$ for $\tilde{a} < \tilde{x} < 1$ is stretched to one of the same type along $\tilde{s} = 0$ for $0 < \tilde{r} < 1$. Finally, the nonhomogeneous Neumann boundary condition as $\tilde{y} \to \infty$ for $0 < \tilde{x} < 1$ corresponds to one of the same type as $\tilde{s} \to \infty$ for $0 < \tilde{r} < 1$. When $\tilde{u}$ is expressed in terms of $(\tilde{r},\tilde{s})$ rather than $(\tilde{x},\tilde{y})$, we denote it by $\tilde{U}(\tilde{r},\tilde{s})$.

The effect of the conformal map on the derivatives within the nonhomogeneous boundary conditions may be evaluated from $\partial\tilde{u}/\partial\tilde{y} = \partial\tilde{U}/\partial\tilde{r} \times \partial\tilde{r}/\partial\tilde{y} + \partial\tilde{U}/\partial\tilde{s} \times \partial\tilde{s}/\partial\tilde{y}$. After manipulation it follows that, along $\tilde{s} = 0$ for $0 < \tilde{r} < 1, \partial\tilde{U}/\partial\tilde{s} = \partial\tilde{u}/\partial\tilde{y} \times f(\tilde{r})$, where

$$f(\tilde{r}) = \frac{\cos\left(\frac{\pi\phi}{2}\right)\sin\left(\frac{\pi\tilde{r}}{2}\right)}{\left[1-\cos^2\left(\frac{\pi\phi}{2}\right)\cos^2\left(\frac{\pi\tilde{r}}{2}\right)\right]^{1/2}} \quad \text{for} \quad 0 < \tilde{r} < 1 \tag{21}$$

and, as $\tilde{s} \to \infty, \partial\tilde{U}/\partial\tilde{s} = \partial\tilde{u}/\partial\tilde{y}$. Eliminating a mixed boundary condition from the problem is of net benefit, but causes $f(\tilde{r})$ to appear in the Robin boundary condition. Finally, defining $\tilde{w}(\tilde{r},\tilde{s}) = \tilde{U}(\tilde{r},\tilde{s}) + (\phi - 1)\tilde{s}$ renders the Neumann boundary condition as $\tilde{s} \to \infty$ homogeneous such that $\nabla^2\tilde{w} = 0$ is subjected to

$$\frac{\partial\tilde{w}}{\partial\tilde{r}} = 0 \quad \text{for} \quad \tilde{r} = 0, \quad \tilde{s} > 0 \tag{22}$$

$$\frac{\partial\tilde{w}}{\partial\tilde{r}} = 0 \quad \text{for} \quad \tilde{r} = 1, \quad \tilde{s} > 0 \tag{23}$$

$$\frac{\partial\tilde{w}}{\partial\tilde{s}} + 1 - \phi = \tilde{h}\left(\tilde{w} + \frac{1}{\tilde{h}}\right)f(\tilde{r}) \quad \text{for} \quad 0 < \tilde{r} < 1, \quad \tilde{s} = 0 \tag{24}$$

$$\frac{\partial\tilde{w}}{\partial\tilde{s}} = 0 \quad \text{for} \quad 0 < \tilde{r} < 1, \quad \tilde{s} \to \infty \tag{25}$$

Solving Eq. (13) by the method of separation of variables and applying the three homogeneous boundary conditions yields

$$\tilde{w} = \sum_{j=0}^{\infty} d_j \cos(j\pi\tilde{r})e^{-j\pi\tilde{s}} \tag{26}$$

Inserting this result into the nonhomogeneous boundary condition (Eq. (24)), multiplying by the jth eigenfunction and integrating across the homogeneous direction, does not yield a direct expression for d_j. However, by expressing the left- and right-hand sides of Eq. (24) in terms of this Fourier series, we can utilize orthogonality to numerically compute d_j.

The function $f(\tilde{r})$ is odd and has a dimensionless period of 4. However, since only its value for $0 < \tilde{r} < 1$ is relevant, we choose to express it in a Fourier cosine series as

$$f(\tilde{r}) = \sum_{k=0}^{\infty} e_k \cos(k\pi\tilde{r}) \tag{27}$$

where standard orthogonality relations yield

$$e_0 = \int_0^1 \frac{\cos\left(\frac{\pi\phi}{2}\right)\sin\left(\frac{\pi\tilde{r}}{2}\right)}{\left[1-\cos^2\left(\frac{\pi\phi}{2}\right)\cos^2\left(\frac{\pi\tilde{r}}{2}\right)\right]^{1/2}}d\tilde{r} \tag{28}$$

$$e_k = 2\int_0^1 \frac{\cos\left(\frac{\pi\phi}{2}\right)\sin\left(\frac{\pi\tilde{r}}{2}\right)}{\left[1-\cos^2\left(\frac{\pi\phi}{2}\right)\cos^2\left(\frac{\pi\tilde{r}}{2}\right)\right]^{1/2}}\cos(k\pi\tilde{r})d\tilde{r} \quad \text{for} \quad k > 0 \tag{29}$$

Analytical results for the preceding integrals are cumbersome. Hence, we compute them numerically.

Utilizing the expression for $\tilde{w}$ (Eq. (26)), the left-hand side of the nonhomogeneous boundary condition (Eq. (24)) may be expressed as

$$\left.\frac{\partial\tilde{w}}{\partial\tilde{s}}\right|_{\tilde{s}=0} + 1 - \phi = \sum_{l=0}^{\infty} f_l \cos(l\pi\tilde{r}) \tag{30}$$

where

$$f_0 = 1 - \phi \tag{31}$$

$$f_l = -l\pi d_l \quad \text{for} \quad k > 0 \tag{32}$$

Moreover, excluding the scaling factor, the right-hand side of this boundary condition may be expressed as

$$\tilde{h}\left[\tilde{w}(\tilde{r},0) + \frac{1}{\tilde{h}}\right] = \sum_{m=0}^{\infty} g_m \cos(m\pi\tilde{r}) \tag{33}$$

where

$$g_0 = \tilde{h}\left(d_0 + \frac{1}{\tilde{h}}\right) \tag{34}$$

$$g_m = d_m\tilde{h} \quad \text{for} \quad k > 0 \tag{35}$$

The product of this Fourier series and that representing the scaling factor (Eq. (21)) equals the Fourier series representation of the left-hand side of the nonhomogeneous boundary condition as per

$$\sum_{l=0}^{\infty} f_l \cos(l\pi\tilde{r}) = \sum_{m=0}^{\infty} g_m \cos(m\pi\tilde{r}) \sum_{k=0}^{\infty} e_k \cos(k\pi\tilde{r}) \tag{36}$$

Multiplying this expression by $\cos(p\pi\tilde{r})$, where p is an integer between 0 and ∞, and integrating across the homogeneous direction yields

$$\sum_{l=0}^{\infty} f_l \int_0^1 \cos(l\pi\tilde{r})\cos(p\pi\tilde{r})d\tilde{r} = \sum_{m=0}^{\infty}\sum_{k=0}^{\infty} g_m e_k \cdot \int_0^1 \cos(m\pi\tilde{r})\cos(k\pi\tilde{r})\cos(p\pi\tilde{r})d\tilde{r} \tag{37}$$

Performing the integration yields a linear system of equations valid between $p=0$ and $p=\infty$ as per

$$\sum_{l=0}^{\infty} f_l t(l,p) = \sum_{m=0}^{\infty}\sum_{k=0}^{\infty} g_m e_k [a(m,k,p) + b(m,k,p) + c(m,k,p) + d(m,k,p)] \tag{38}$$

where

$$t(l,p) = \begin{cases} 1 & \text{if } l=p=0 \\ 1/2 & \text{if } l=p>0 \\ 0 & \text{otherwise} \end{cases} \tag{39}$$

$$a(m,k,p) = \begin{cases} 1/4 & \text{if } m=k=p=0 \\ 0 & \text{otherwise} \end{cases} \tag{40}$$

$$b(m,k,p) = \begin{cases} 1/4 & \text{if } k-m=p \\ 0 & \text{otherwise} \end{cases} \tag{41}$$

$$c(m,k,p) = \begin{cases} 1/4 & \text{if } m+k=p \\ 0 & \text{otherwise} \end{cases} \tag{42}$$

$$d(m,k,p) = \begin{cases} 1/4 & \text{if } m-k=p \\ 0 & \text{otherwise} \end{cases} \tag{43}$$

Upon removal of the terms equal to zero in the sum and double sum in Eq. (38), it becomes

$$f_0 = e_0 g_0 + \frac{1}{2}\sum_{m=1}^{\infty} e_m g_m \quad (p=0) \tag{44}$$

$$2f_p = \sum_{m=0}^{p} e_{p-m} g_m + \sum_{m=0}^{\infty} e_m g_{m+p} + e_{m+p} g_m \quad (p \geq 1) \tag{45}$$

The unknown column vector in the linear system, d_j, appears in f_l (for $l \geq 1$) and g_m (for all m). We impose $P+1$ unknowns (d_0 through d_P) on a truncated form of the linear system with $P+1$ equations (those for $p=0$ through $p=P$) by truncating the sums therein according to

$$f_0 = g_0 e_0 + \frac{1}{2}\sum_{m=1}^{P} e_m g_m \quad (p=0) \tag{46}$$

$$2f_p = \sum_{m=0}^{p} e_{p-m} g_m + \sum_{m=0}^{P-p} e_m g_{m+p} + \sum_{m=0}^{P} e_{m+p} g_m \quad (p \geq 1) \tag{47}$$

The linear systems were solved using the built-in lower upper factorization from MATLAB to find the coefficients, d_j, although we note that an indirect method, using a few steps of Gauss–Seidel iteration, gave effectively the same results. Evaluation of the thermal slip length requires an expression for $\theta(\tilde{x},0)$ along $\tilde{y}=0$. Upon transforming from $\tilde{w}$ back to θ, it follows that

$$\theta(\tilde{x},0) = \sum_{j=0}^{P} d_j \cos[j\pi\tilde{r}(\tilde{x},0)] e^{-j\pi\tilde{s}(\tilde{x},0)} + (1-\phi)\tilde{s}(\tilde{x},0) \tag{48}$$

where it follows from Eq. (19) and the requirement that $\tilde{s}(\tilde{x},0) \geq 0$ that for $0 \leq \tilde{x} \leq 1$:

$$\tilde{r}(\tilde{x},0) = \frac{2}{\pi}\cos^{-1}\left[\frac{\cos\left(\frac{\pi}{2}\tilde{x}\right)}{\cos\left(\frac{\pi}{2}\phi\right)}\right] H(\tilde{x}-\phi) \tag{49}$$

$$\tilde{s}(\tilde{x},0) = -\frac{2}{\pi}\ln\left[\frac{\cos\left(\frac{\pi}{2}\tilde{x}\right)}{\cos\left(\frac{\pi}{2}\phi\right)} - \left|\sqrt{\frac{\cos^2\left(\frac{\pi}{2}\tilde{x}\right)}{\cos^2\left(\frac{\pi}{2}\phi\right)} - 1}\right|\right] H(\phi-\tilde{x}) \tag{50}$$

where H is the Heaviside step function, which equals 0 and 1 when its argument is <0 and ≥ 0, respectively. Noting that

$$\phi = -\left.\frac{\partial\bar{\theta}}{\partial\tilde{y}}\right|_{\mathrm{c}} \tag{51}$$

the definition of thermal slip length implies that

$$\tilde{b}_{\mathrm{t}} = \frac{1-\phi}{2\phi^2}\int_0^{\phi}\theta(\tilde{x},0)d\tilde{x} - \frac{1}{2\phi}\int_{\phi}^{1}\theta(\tilde{x},0)d\tilde{x} \tag{52}$$

We compute $\tilde{b}_{\mathrm{t}}$ for prescribed values of ϕ and $\tilde{h}$ by setting $P=200$ and increasing it by 200 until no change is observed in the result to six digits.

2.3 Isothermal Meniscus. The boundary conditions for an isoflux solid–liquid interface and isothermal meniscus are those given by Eqs. (14)–(18), except that Eq. (15) is replaced by $\theta=0$ for $\phi<\tilde{x}<1$ and $\tilde{y}=0$. The solution is the superposition of those to a one-dimensional background problem and a two-dimensional perturbation problem. The former is governed by $d^2\theta_{1\mathrm{D}}/d\tilde{y}^2=0$ subjected to $\theta_{1\mathrm{D}}=0$ at $\tilde{y}=0$ and $d\theta_{1\mathrm{D}}/d\tilde{y}=-\phi$ as $\tilde{y}\to\infty$ such that $\theta_{1\mathrm{D}}=-\phi\tilde{y}$. The latter is governed by $\nabla^2\theta_p=0$ subjected to the symmetry boundary conditions and

$$\frac{\partial\theta_p}{\partial\tilde{y}} = \phi-1 \quad \text{for} \quad 0<\tilde{x}<\tilde{a}, \quad \tilde{y}=0 \tag{53}$$

$$\theta_p = 0 \quad \text{for} \quad \tilde{a}<\tilde{x}<1, \quad \tilde{y}=0 \tag{54}$$

$$\frac{d\theta_p}{d\tilde{y}} = 0, \quad \text{for} \quad 0<\tilde{x}<1, \quad \tilde{y}\to\infty \tag{55}$$

We note that $\bar{\theta}_{\mathrm{sl}} - \theta_{\tilde{y}\to\infty} = \left(\theta_{1\mathrm{D},\tilde{y}=0} - \theta_{1\mathrm{D},\tilde{y}\to\infty}\right) + \left(\bar{\theta}_{p,\mathrm{sl}} - \theta_{p,\tilde{y}\to\infty}\right)$ and that $\theta_{1\mathrm{D},\tilde{y}=0} - \theta_{1\mathrm{D},\tilde{y}\to\infty} = \bar{\theta}_{\mathrm{c}} - \theta_{\tilde{y}\to\infty}$. Then, it follows from Eq. (2) that the thermal slip length is

$$\tilde{b}_{\mathrm{t}} = \frac{\bar{\theta}_{p,\mathrm{sl}} - \theta_{p,\tilde{y}\to\infty}}{2(\partial\theta/\partial\tilde{y})|_{\mathrm{c}}} \tag{56}$$

Philip [18] solved a mathematically equivalent perturbation problem in the context of shear flow over a plate with a regular array of shear-free slots parallel to the flow direction. Utilizing his results in Eq. (56), the thermal slip length becomes

$$\tilde{b}_{\mathrm{t}} = \frac{(1-\phi)}{\pi\phi}\left\{\frac{1}{\phi}\int_0^{\phi}\cosh^{-1}\left[\sec\left(\frac{\pi\phi}{2}\right)\cos\left(\frac{\pi\tilde{x}}{2}\right)\right]d\tilde{x} - \ln\left[\sec\left(\frac{\pi\phi}{2}\right)\right]\right\} \tag{57}$$

3 Model Verification

To verify the analytical results, STAR-CCM+® version 7.04 (double precision) was used to solve the problem for an adiabatic meniscus, an isothermal meniscus, and three finite nondimensional heat transfer coefficient values at the meniscus, i.e., $\tilde{h}=1100$, and 1000, all at solid fractions of 0.01 and 0.1. The height of the computational domain was set to 25 times the structure pitch to well approximate a semi-infinite domain. A finite volume approach with an algebraic multigrid iterative solver was employed. The meshes utilized featured increasing levels of refinement near the solid–liquid interface, where steep

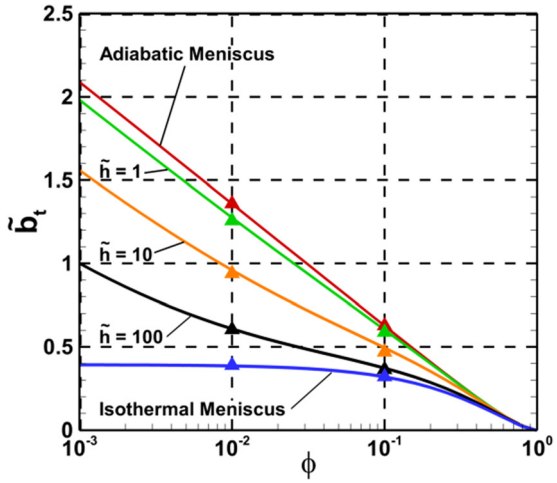

Fig. 3 Dimensionless thermal slip length versus solid fraction for adiabatic meniscus, finite dimensionless heat transfer coefficient at meniscus and isothermal meniscus when the boundary condition at the solid–liquid interface is constant heat flux. Triangles correspond to numerical verification of semi-analytical solution method.

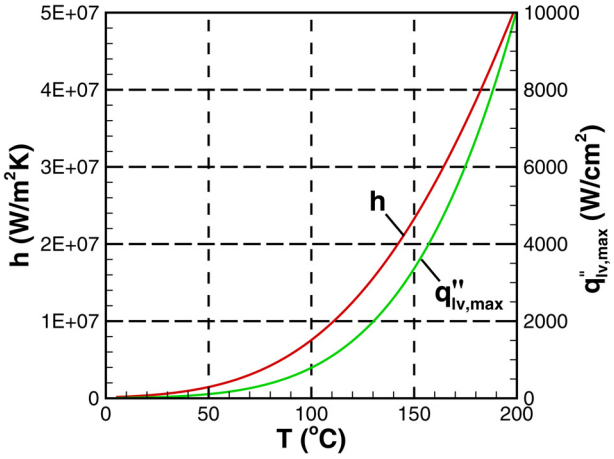

Fig. 4 Interfacial heat transfer coefficient and maximum interfacial heat flux to which it applies as a function of temperature for water

temperature gradients were present. Meshes were generated for both solid fractions and were subsequently refined until the thermal slip length for the isothermal meniscus case was within 1% of the analytical value given by Eq. (57). To further confirm the validity of the meshes, the meniscus was also subjected to the adiabatic condition and the resulting thermal slip lengths agreed with the analytical predictions (Eq. (3)) to within 0.04%. The meshes used for $\phi = 0.1$ and 0.01 contained nominally 200 k and 370 k cells, respectively. Further refinement to the smaller solid fraction mesh for the adiabatic meniscus case yielded a change in thermal slip length of less than 0.02%. The solutions were deemed converged, when the norm of the residual of the discretized Laplace equations approached its asymptotic value of nominally 10^{-13} and, within numerical precision, the thermal slip length ceased to change.

4 Results

The semi-analytically computed thermal slip length is plotted versus solid fraction for an adiabatic meniscus, selected finite values of dimensionless heat transfer coefficient, and an isothermal meniscus in Fig. 3. The corresponding numerical results for the aforementioned discrete values of ϕ and $\tilde{h}$ are shown by the solid triangles. The mean of the absolute value of the discrepancy between the analytical and numerical results is 1.61%.

As discussed by Carey [19], Schrage [20] derived an expression for the interfacial heat transfer coefficient as per

$$h = \frac{2\hat{\sigma}}{2-\hat{\sigma}} \frac{h_{lv}^2}{\bar{T}_{lv} v_{lv}} \left(\frac{M}{2\pi R \bar{T}_{lv}}\right)^{1/2} \left(1 - \frac{p_v v_{lv}}{2h_{lv}}\right) \tag{58}$$

where properties are evaluated at $\bar{T}_{lv}$ and $\hat{\sigma}$ is the accommodation coefficient, h_{lv} is the latent heat of evaporation, v_{lv} is the difference between saturated vapor and saturated liquid specific volumes, M is the molecular weight of the liquid, R is the universal gas constant and p_v is saturation pressure. Equation (58) is valid when

$$\frac{q''_{lv}}{\rho_v h_{lv}} \left(\frac{2R\bar{T}_{lv}}{M}\right)^{1/2} \leq 0.01 \tag{59}$$

where ρ_v is the vapor density. When the right-hand side of this equation equals 0.01, the corresponding interfacial heat flux is denoted by $q''_{lv,max}$. Equation (58) imposes a linear relationship between the (local) heat flow and the (local) temperature difference between the phases. This implies that conditions are sufficiently close to equilibrium such that the Boltzmann distribution describes the velocity distribution of vapor molecules leaving and approaching the meniscus. In the case of water, assuming an accommodation coefficient of unity, the extremely high interfacial heat transfer coefficient and corresponding $q''_{lv,max}$ are plotted versus temperature in Fig. 4 based upon the properties of water in Ref. [21]. When Eq. (59) is invalid, Schrage [20] provides a more cumbersome relation to compute the interfacial heat transfer coefficient.

Thermal slip length is computed by prescribing ϕ and $\bar{T}_{lv}$ using Fig. 4 to determine the corresponding value of $\tilde{h}$ and finding b_t from Fig. 3. For example, for $\phi = 0.01$ and $\bar{T}_{lv} = 100\,^{\circ}\mathrm{C}$, in the case of water, $h = 7.55 \times 10^6 \mathrm{W/(m^2 \cdot K)}$ and $q''_{lv,max} = 792 \mathrm{W/cm^2}$. Assuming a ridge pitch of 2 μm ($d = 1$ μm), $\tilde{h} = 11.12$ and $\tilde{b}_t = 0.94$, which is a 30% reduction relative to the case of an adiabatic meniscus and 2.44 times the limiting value for an isothermal meniscus. Macroscopically, the Nusselt number is a function of the thermal slip length [7] and its value computed from the analysis herein rather than that for an adiabatic meniscus should be utilized.

5 Conclusions

We developed expressions for the dimensionless (apparent) thermal slip length for liquid flow in the Cassie state over ridge-type structured surfaces in the presence of local evaporation and condensation along the meniscus subject to the constraint that the net rate of phase change is zero. An isoflux boundary condition was imposed at the solid–liquid interface. In the limiting case of an isothermal meniscus, analytical results provide thermal slip length as a function of solid fraction. In the case of a finite heat transfer coefficient along the meniscus, semi-analytical results provide thermal slip length as a function of solid fraction and dimensionless interfacial heat transfer coefficient. Evaporation and condensation substantially reduce thermal slip lengths at conditions relevant to water-based thermal management of electronics. The reduction in thermal resistance of a microchannel heat sink may be quantified by using apparent thermal slip lengths computed from the present analysis in relevant Nusselt number expressions. Future work should consider the effect of evaporation and condensation on the hydrodynamic slip length as they induce a nonzero velocity normal to the meniscus. More rigorous expressions for both slip lengths in diabatic flows must simultaneously account for the effects of curvature, thermocapillary stress, and evaporation and condensation along the meniscus and, as per the

study by Ng and Wang [10], relax the assumption that heat is supplied to the fluids exclusively at the solid–liquid interface.

Acknowledgment

The authors gratefully acknowledge Durwood Marshall and Shawn Doughty of Tufts Technology Services for their assistance and access to Tufts UIT Research Computing facilities. We acknowledge Bruce Bogosian for a useful discussion on the solution of Laplace's equation subjected to mixed boundary conditions. Bell Labs Ireland thanks the Industrial Development Agency (IDA) Ireland for their financial support. Funding for this research was provided in part by NSF CBET Award No. 1402783.

Nomenclature

a = half width of ridge (m)
b = apparent hydrodynamic slip length (m)
b_t = apparent thermal slip length (m)
c_p = specific heat at constant pressure (J/(kg K))
d = half pitch of ridges (m)
$\tilde{D}$ = mapped distance along ridge
h = interfacial heat transfer coefficient (W/(m^2 K))
$\tilde{h}$ = dimensionless interfacial heat transfer coefficient
h_{lv} = latent heat of evaporation
H = Heaviside step function
k = thermal conductivity (W/(m K)), index
m = index
$\dot{m}$ = mass flow rate (kg/s)
M = molecular weight
p = index
P = maximum index value
p_v = saturation pressure (N/m^2)
Pe_c = Péclet number based on the length scale of the composite interface
q'' = heat flux (W/m^2)
$\tilde{r}$ = imaginary coordinate
R = universal gas constant (8.3144 kJ/(kg mol K))
Re_c = Reynolds number based on the length scale of the composite interface
$\tilde{s}$ = imaginary coordinate
T = temperature (K)
U = mapped temperature (K)
$\tilde{u}$ = temperature (K)
$\tilde{v}$ = conformal map
v_{lv} = difference between saturated vapor and saturated liquid specific volumes (m^3/kg)
w = streamwise velocity (m/s)
$\tilde{w}$ = mapped temperature (K)
x = lateral coordinate parallel to composite interface
y = spanwise coordinate normal to composite interface
z = streamwise coordinate
$\tilde{z}$ = complex coordinate

Greek Symbols

ϕ = solid fraction
μ = viscosity (kg/s m)
ρ = density (kg/m^3)
$\hat{\sigma}$ = accommodation coefficient

Symbols

$\bar{}$ = mean quantity
$\tilde{}$ = dimensionless quantity

Subscripts

c = composite interface
lv = liquid–vapor
m = bulk or mean quantity
sl = solid–liquid
v = vapor

References

[1] Quéré, D., 2005, "Non-Sticking Drops," Rep. Prog. Phys., **68**(11), pp. 2495–2532.
[2] Steigerwalt Lam, L., Hodes, M., and Enright, R., 2015, "Analysis of Galinstan Based Microgap Cooling Enhancement in the Presence of Apparent Slip," ASME J. Heat Transfer (in press).
[3] Hodes, M., Kolodner, P., Krupenkin, T., Lee, W., Lyons, A., Salamon, T., Taylor, J., and Weiss, D., 2007, "Techniques for Microchannel Cooling," U.S. Patent No. 7,204,298.
[4] Navier, C., 1823, "Mémoire Sur Les Lois du Mouvement Des Fluides," Mémoires de l'Acad. R. Sci. Inst. Fr., **6**, pp. 389–440.
[5] Lauga, E., and Stone, H. A., 2003, "Effective Slip in Pressure-Driven Stokes Flow," J. Fluid Mech., **489**, pp. 55–77.
[6] Davis, A., and Lauga, E., 2010, "Hydrodynamic Friction of Fakir-Like Superhydrophobic Surfaces," J. Fluid Mech., **661**, pp. 402–411.
[7] Enright, R., Hodes, M., Salamon, T., and Muzychka, Y., 2013, "Isoflux Nusselt Number and Slip Length Formulae for Superhydrophobic Microchannels," ASME J. Heat Transfer, **136**(1), p. 012402.
[8] Ybert, C., Barentin, C., Cottin-Bizonne, C., Joseph, P., and Bocquet, L., 2007, "Achieving Large Slip With Superhydrophobic Surfaces: Scaling Laws for Generic Geometries," Phys. Fluids, **19**(12), p. 123601.
[9] Yovanovich, M., 1998, "Conduction and Thermal Contact Resistances (Conductances)," *Handbook of Heat Transfer*, 3rd ed., W. Rohsenow, and J. H. Y. Cho, eds., McGraw-Hill, New York.
[10] Ng, C.-O., and Wang, C. Y., 2014, "Temperature Jump Coefficient for Superhydrophobic Surfaces," ASME J. Heat Transfer, **136**(6), p. 064501.
[11] Maynes, D., and Crockett, J., 2013, "Apparent Temperature Jump and Thermal Transport in Channels With Streamwise Rib and Cavity Featured Superhydrophobic Walls at Constant Heat Flux," ASME J. Heat Transfer, **136**(1), p. 011701.
[12] Cowley, A., Maynes, D., and Crockett, J., 2014, "Effective Temperature Jump Length and Influence of Axial Conduction for Thermal Transport in Superhydrophobic Channels," Int. J. Heat Mass Transfer, **79**, pp. 573–583.
[13] Steigerwalt Lam, L., Melnick, C., Hodes, M., Ziskind, G., and Enright, R., 2014, "Nusselt Numbers for Thermally Developing Couette Flow With Hydrodynamic and Thermal Slip," ASME J. Heat Transfer, **136**(5), p. 051703.
[14] Jiji, L., 2009, *Heat Convection*, Springer, Berlin.
[15] Duan, Z., and Muzychka, Y., 2010, "Slip Flow in the Hydrodynamic Entrance Region of Circular and Noncircular Microchannels," ASME J. Fluids Eng., **132**(1), p. 011201.
[16] Colin, S., 2012, "Gas Microflows in the Slip Flow Regime: A Critical Review on Convective Heat Transfer," ASME J. Heat Transfer, **134**(2), p. 020908.
[17] Rothstein, J. P., 2010, "Slip on Superhydrophobic Surfaces," Annu. Rev. Fluid Mech., **42**(1), pp. 89–109.
[18] Philip, J. R., 1972, "Flows Satisfying Mixed No-Slip and No-Shear Conditions," J. Appl. Math. Phys. (ZAMP), **23**, pp. 353–372.
[19] Carey, V. P., 1992, *Liquid–Vapor Phase-Change Phenomena*, Hemisphere, New York.
[20] Schrage, R. W., 1953, *A Theoretical Study of Interphase Mass Transfer*, Columbia University Press, New York.
[21] Lemmon, E., McLinden, M., and Friend, D., 2011, "Thermophysical Properties of Fluid Systems," *NIST Chemistry WebBook, NIST Standard Reference Database Number 69*, P. Linstrom, and W. Mallard, eds., National Institute of Standards and Technology, Gaithersburg, MD.